Materials Science Forum
ISSN: 1662-9752, Vol. 1062, pp 38-43
doi:10.4028/p-sg9dq0

Submitted: 2021-10-14
Revised: 2022-02-08
Accepted: 2022-02-24
Online: 2022-05-31

Aluminum Activation in 4H-SiC Measured on Laterally Contacted MOS Capacitors with a Buried Current-Spreading Layer

Kristijan Luka Mletschnig[1,a*], Mathias Rommel[2,b], Gregor Pobegen[3,c], Werner Schustereder[1,d] and Peter Pichler[2,e]

[1]Infineon Technologies Austria AG, Siemensstraße 2, 9500 Villach, Austria

[2]Fraunhofer Institute for Integrated Systems and Device Technology IISB, Schottkystraße 10, 91058 Erlangen, Germany

[3]KAI Kompetenzzentrum Automobil- und Industrieelektronik GmbH, Europastraße 8, 9524 Villach, Austria

[a]KristijanLuka.Mletschnig@infineon.com, [b]Mathias.Rommel@iisb.fraunhofer.de, [c]Gregor.Pobegen@k-ai.at, [d]Werner.Schustereder@infineon.com, [e]Peter.Pichler@iisb.fraunhofer.de

Keywords: aluminum implantation, electrical activation, p-type, 4H-SiC, MOS capacitor, capacitance voltage

Abstract. The excellent material properties of the wide band gap semiconductor SiC are accompanied by challenges in device processing. Of particular importance is the incomplete activation of implanted Al acceptors after high-temperature annealing. In this work, we present a novel approach in applying the differential-capacitance method to lateral MOS capacitors, where systematic errors in its characterization are reduced by introducing a buried current-spreading layer. We find that the implantation of an additional current-spreading layer significantly reduces series resistance effects and enables a reliable capacitance-voltage measurement of low dopant concentrations of p-type wells in n-type epitaxial layers. The measurement of an Al box-like profile implanted at 500 °C and resulting in a doping concentration of $3 \cdot 10^{17}$ cm^{-3} shows full activation after annealing at 1800 °C for 30 minutes.

Introduction

The aluminum acceptors in SiC were reported to be incompletely activated whereby the activation degree depends on the implanted dopant concentration, annealing temperature, and annealing time [1]. Dopant activation in 4H-SiC is typically derived from Hall measurements [2], though this method requires high sample temperatures due to the rather high ionization energy of Al. Besides, the method still leaves room for ambiguities since the Hall scattering factor is significantly less established for implanted high dopant concentrations than for low-concentration epitaxial layers [3] despite recent thorough investigations [4].

Another standard method to determine activation at room temperature used also in our work is the direct measurement of the net active dopant concentration $N_{Al} - N_D$ within a space-charge region (SCR) via capacitance-voltage (C-V) measurements [5, 6] as determined by equation 1, with elementary charge q, contact area A, dielectric constant ε_0 and relative permittivity ε_r.

$$N_{Al} - N_D = \frac{2}{q\varepsilon_r\varepsilon_0 A^2 \, d\left(\frac{1}{C^2}\right)/dV}. \tag{1}$$

For SiC, this approach was e.g. demonstrated for p-type epitaxial layers on p-type substrates using Schottky barrier diodes in vertical configuration [7] or using mercury probes in vertical and lateral configuration [8]. In order to facilitate a direct characterization of p-type implanted and annealed areas in n-type epitaxial layers on n-type substrates we fabricated planar MOS capacitors with laterally contacted p-wells (Fig. 1) [9].

The equivalent circuit of this setup is assumed to consist of a capacitor with capacitance C, which is to be determined, with an Ohmic parallel conductance G, as well as a series resistor with resistance r_s, as depicted in Fig. 1. The measured quantities, in turn, are the capacitance C_P and conductance G_P in parallel circuit, which depend on the angular probe frequency ω. The components of both equivalent circuits are related to each other via equations 2a and 2b:

$$C_P = \frac{C}{(1 + r_s G)^2 + (\omega r_s C)^2}, \quad G_P = \frac{G(1 + r_s G) + r_s(\omega C)^2}{(1 + r_s G)^2 + (\omega r_s C)^2}. \tag{2a, 2b}$$

Thus, measuring the capacitance assuming a parallel C_P G_P equivalent circuit, the capacitance decreases for high AC frequencies with increasing series resistance r_s. To determine the frequency-independent true capacitance C, the condition $\omega r_s C \ll 1$ must be fulfilled [10]. For low Al acceptor concentrations in SiC (as e.g. in p-type implanted wells in n-type epitaxial layers) the series resistance can become critical, especially for large contact areas. Furthermore, depending on the p- and n-type concentrations, the voltage-dependent SCR of the MOS capacitor can extend up to the intrinsic SCR of a p-well's p-n-junction, leading to a full or partial pinch-off in the conductive channel between the SCRs, causing a voltage dependent r_s [11].

To reduce r_s and prevent a pinch-off, we implanted and annealed a buried Al layer of moderate concentration below the Al box-like profile, acting as a current-spreading layer during the capacitance measurement (Fig. 1). To further reduce r_s, the annular p^+ contact implantation was extended in depth to connect the current-spreading layer.

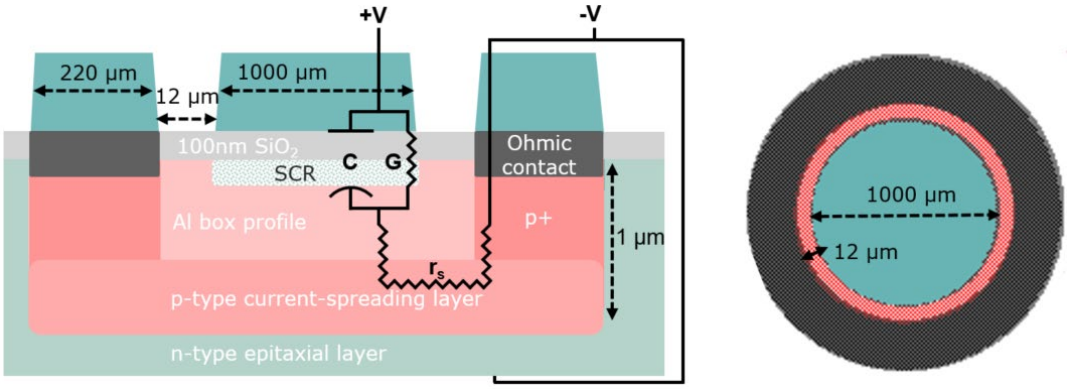

Fig. 1 Cross-sectional (left) and top view (right) of a lateral MOS capacitor with an annular Ohmic contact ring, current-spreading layer and vertically extended contact implantation, including the schematics of the proposed equivalent circuit. Sketch is not to scale.

Experimental Details

Lateral MOS capacitors were processed on n-type 4H-SiC substrates with a $1 \cdot 10^{16}$ cm^{-3} nitrogen-doped epitaxial layer. An Al box-like profile with a $3 \cdot 10^{17}$ cm^{-3} plateau concentration was implanted through a 50 nm stray oxide at 500 °C. The profile consists of multiple energy implantations with parameters presented in Table 1. This Al well was implanted through a circular opening with a diameter of about 1460 µm in an SiO_2 mask structured by plasma etching. Additionally, in part of the samples Al was implanted at 500 °C with an energy of 900 keV to a peak concentration of $1 \cdot 10^{19}$ cm^{-3} to form a current-spreading layer.

Table 1: Implantation parameters for the Al box-like profiles with optional current-spreading layer.

Energy [keV]	30	50	75	105	145	200	300	900
Dose [cm^{-2}] $3 \cdot 10^{17}$ cm^{-3}	$5.4 \cdot 10^{11}$	$7.5 \cdot 10^{11}$	$9.0 \cdot 10^{11}$	$1.2 \cdot 10^{12}$	$1.6 \cdot 10^{12}$	$2.3 \cdot 10^{12}$	$5.4 \cdot 10^{12}$	$2.4 \cdot 10^{14}$
Dose [cm^{-2}] $1 \cdot 10^{20}$ cm^{-3}	$1.8 \cdot 10^{14}$	$2.5 \cdot 10^{14}$	$3.0 \cdot 10^{14}$	$4.0 \cdot 10^{14}$	$5.2 \cdot 10^{14}$	$7.6 \cdot 10^{14}$	$1.8 \cdot 10^{15}$	/

A contact-implantation ring with a width of 220 µm and a box-like depth profile with a plateau concentration of $1 \cdot 10^{20}$ cm^{-3} was implanted at 500 °C into the outer rim (see Table 1 for the implantation parameters). This high-concentration profile extends towards the current-spreading layer, as schematically depicted in Fig. 1.

Following the removal of the oxide mask, the wafer was protected with graphite. After activation annealing at 1800 °C for 30 minutes, the graphite capping layer was removed and a 100 nm TEOS oxide was deposited and densified, later acting as oxide layer in the MOS structure. A Ni silicide Ohmic contact ring was formed in the contact regions via rapid thermal processing. A 1 µm thick Al top-metallization was then deposited on the Ti/TiN liners and structured such that the central contact pad has a diameter of about 1000 µm and a distance to the Ohmic contact ring of about 12 µm. Ni silicide backside Ohmic contacts were formed by thermal annealing.

The capacitance-voltage characteristics were measured with an Agilent 4294A precision impedance analyzer. The p-well is inherently isolated from the n-type epitaxial layer through the intrinsic p-n-junction. To keep the SCR of the p-n-junction unbiased, the annular contact of the lateral MOS capacitor and the backside contact to the n-type substrate were kept at the same potential, as indicated in Fig. 1.

Results and Discussion

To determine the series resistance r_s, the frequency-dependent capacitance $C_P(f)$ and conductance $G_P(f)$ were measured on two neighboring MOS capacitors on a single wafer, one with and one without current-spreading layer with an AC-amplitude of 100 mV. From fitting equation 2b to $G_P(f)$, the actual conductance G was found to be below 0.1 µS/cm^2 at 0 V DC-bias in both samples (Fig. 2a). The series resistance is then determined by applying a non-linear least square optimizing function for equation 2b to the experimental $C_P(f)$ data, as shown in Fig. 2b. The capacitance C at 0 V DC-bias is about 19 nF/cm^2 for both samples.

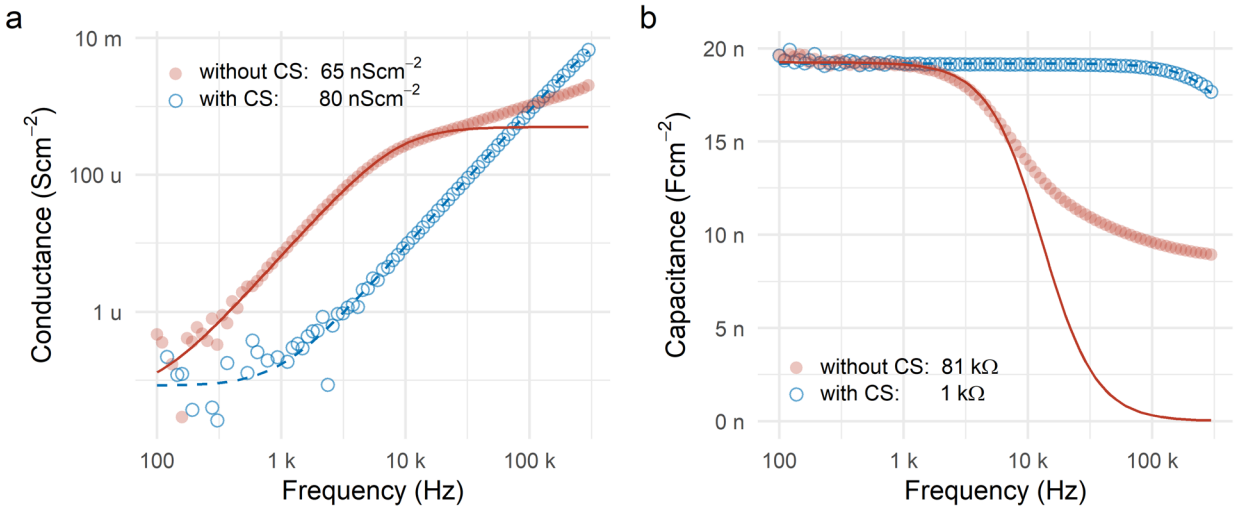

Fig. 2 a) Conductance-frequency dependence $G_P(f)$ and b) capacitance-frequency dependence $C_P(f)$ at 0 V DC-bias for samples with (blue empty circles) and without (red dots) current-spreading layer. Dots denote the experimental data, lines correspond to the numerical fit. The legends include the fitted conductance and series resistance values, respectively.

We find from Fig. 2b that introducing a current-spreading layer significantly reduces the series resistance from about 81 kΩ to about 1 kΩ. Moreover, the experimental data cannot be adequately described for the sample without current-spreading layer in the whole frequency range within the parallel equivalent circuit model with a series resistor. We attribute the discrepancies to the influence of parasitic components on C_P, such as serial capacitances or inductances. Therefore, the data taken into account for fitting were limited to 10 kHz for the latter sample.

To conclusively relate the capacitance's frequency dependence to the series resistance, we have investigated its temperature dependence for the sample with a current-spreading layer (Fig. 3a). We found that r_s decreases with increasing temperature, characterized by a slope of 128 meV in an Arrhenius plot evaluation (Fig. 3b). This corresponds well to the reported ionization energy of Al for a concentration of about $1 \cdot 10^{19}$ cm^{-3} [12] and is consistent with a series resistance that is predominantly determined by the current-spreading layer.

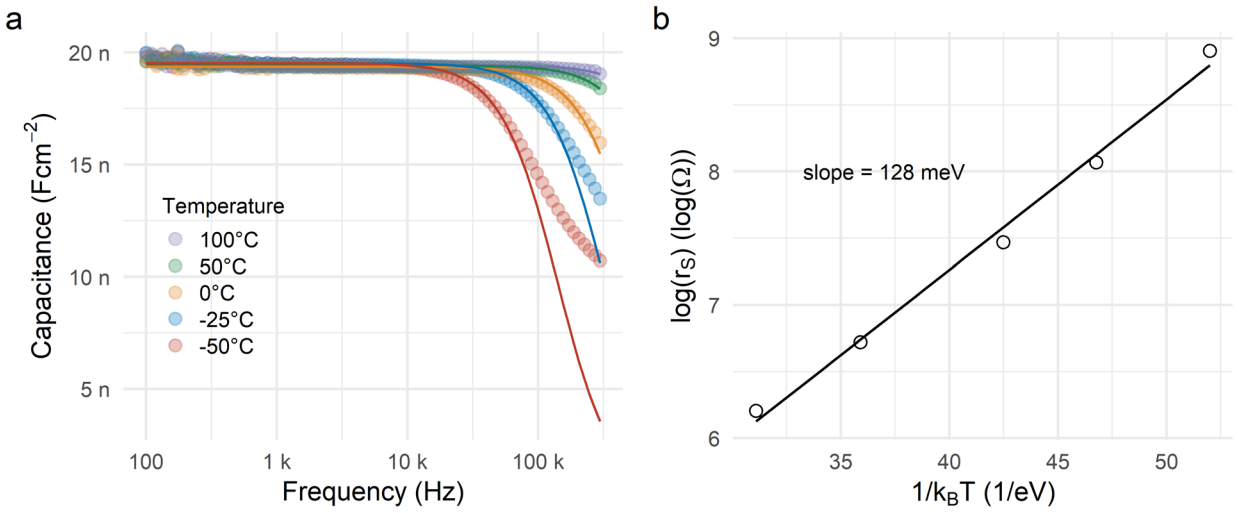

Fig. 3 a) Capacitance-frequency dependence at 0 V DC-bias for the sample with a current-spreading layer measured at different temperatures. b) Arrhenius representation of the series resistance determined from fitting the $C_P(f)$ data.

With the r_s values found from fitting the experimental data at 0 V DC-bias shown in Fig. 2b, the condition $\omega r_s C \ll 1$ at a typical AC probe frequency of 100 kHz is only fulfilled for the sample with a current-spreading layer ($\omega r_s C \sim 0.05$). For the sample without a current-spreading layer, the probe frequency had to be reduced to 1 kHz. For both samples, capacitance and series resistance were evaluated from -40 V accumulation bias towards 40 V depletion bias (Fig. 4a).

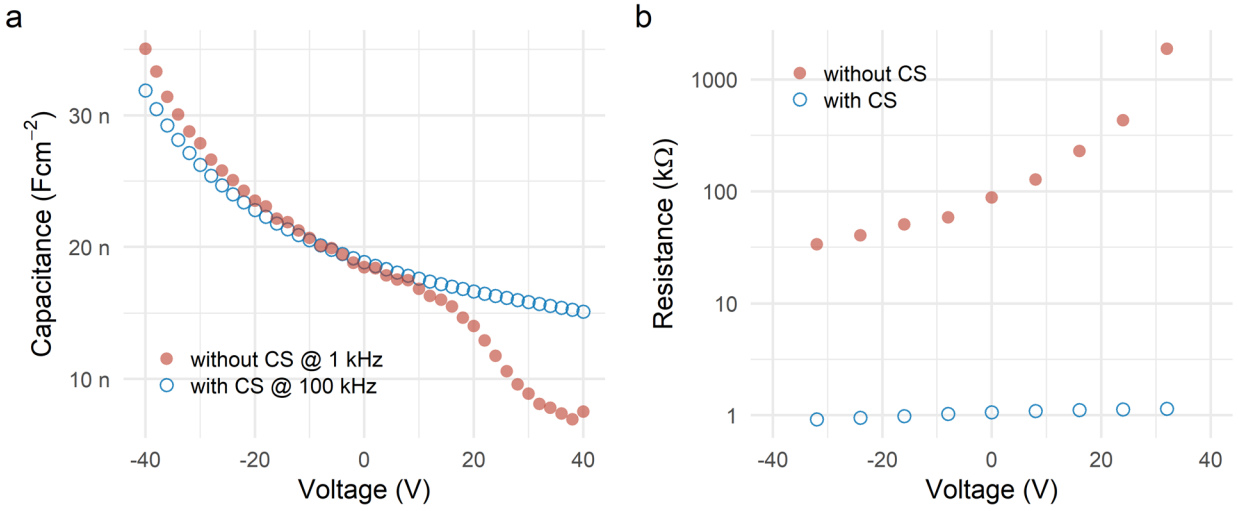

Fig. 4 a) The C-V data for -40 V accumulation towards 40 V depletion bias at 100 kHz and 1 kHz for the sample with and without a current-spreading layer, respectively. b) The series resistance as a function of applied voltage determined from $C_P(f)$ data.

In both samples, the capacitance decreases with voltage as the SCR is expanding. However, for the sample without a current-spreading layer, the measured capacitance drops below the capacitance value of the sample including a current-spreading layer for voltages exceeding 5 V.

By determining the series resistance from measuring $C_P(f)$ it is revealed that r_s diverges with increasing voltage in the sample without a current-spreading layer, whereas it increases only slightly for the sample including a current-spreading layer (Fig. 4b). We attribute the drastic increase in series resistance in the sample without a current-spreading layer to a pinch-off in the conductive channel between the SCRs of the p-well and p-n-junction. This is supported by the estimated width of the p-well's SCR of about 380 nm at 40 V depletion bias, which would extend throughout the whole profile in case that no current-spreading layer is present.

The C-V data were used to determine the net dopant concentration via the differential-capacitance method [5]. For the sample including a current-spreading layer, the detected net dopant concentration is about $3 \cdot 10^{17}$ cm^{-3} at lower bias voltages, showing a slight increase of the concentration with depth (Fig. 5). This increase in concentration is supported by SIMS measurements and can be attributed to the tail region of the implanted current-spreading layer. Overall, a stable profile can be obtained owing to the high AC probe frequency of 100 kHz.

In contrast, when measuring the sample without a current-spreading layer, the resulting profile is noisy due to the lower probe frequency of 1 kHz, which could be overcome by increasing the measurement time. However, the dopant concentration is significantly underestimated above 5 V depletion bias as a result of the pinch-off in the conductive channel between the SCRs of the p-well and p-n-junction (Fig. 5).

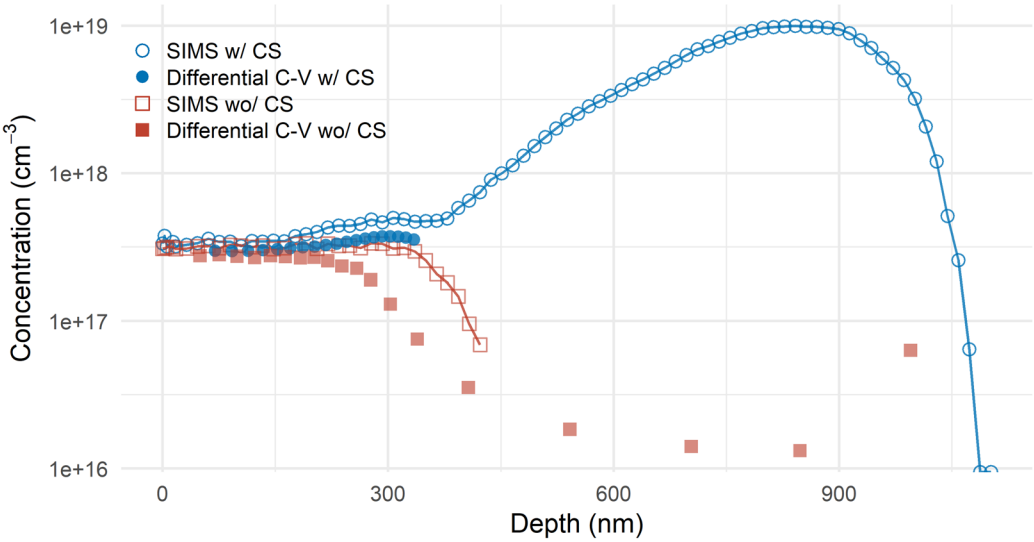

Fig. 5 SIMS profiles (open symbols) compared to profiles derived from the differential-capacitance method (full symbols) for the samples with and without current-spreading layer.

The dopant concentration derived from SIMS measurements agrees well with the net dopant concentration of the sample with a current-spreading layer, which implies full dopant activation for a dopant concentration of $3 \cdot 10^{17}$ cm^{-3} after annealing at 1800 °C for 30 minutes. These results are in good agreement with previously reported activation degrees derived from mercury probe measurements [8]. However, recent Hall-measurements of Al-implanted samples in a comparable concentration range ($1 \cdot 10^{17}$ - $5 \cdot 10^{17}$ cm^{-3}) suggest a compensation ratio of about 30% [13], which is not apparent in our data. Hall measurements of the sample without a current-spreading layer are pending to investigate this dissent.

Summary

In conclusion, we have demonstrated that the activation of low-concentration Al implanted p-wells in n-type 4H-SiC can be determined on lateral MOS capacitors with reduced series resistance by introducing a buried current-spreading layer. The experimental data on the capacitance-frequency dependence $C_P(f)$ agree well with the parallel equivalent circuit model.

The temperature dependence of r_s for the sample with a current-spreading layer follows an Arrhenius law with a slope of about the ionization energy of 10^{19} cm^{-3} Al, which is consistent with a series resistance determined predominantly by the current-spreading layer.

Depending on the series resistance, the AC probe frequency needs to be adjusted following the condition $\omega r_s C \ll 1$ to accurately measure the capacitance voltage characteristics. If the condition is not met due to a high series resistance, the dopant concentration derived from differential capacitance measurements can be severely underestimated. Although introducing a current-spreading layer alters the underlying dopant profile, it could in principle be implanted deeper below the profile to be investigated.

Finally, we report that aluminum with a concentration of $3 \cdot 10^{17}$ cm^{-3} implanted at 500 °C reaches full activation after annealing at 1800 °C for 30 minutes. To investigate the discrepancy to reported compensation ratios of about 30 % in this concentration regime, Hall-measurements are to be performed on the samples used in this work.

Since the capacitance-voltage method worked very well in the regime of low Al concentrations, we expect that the presented setup is also a promising method for investigating higher dopant concentrations and different doping species.

Acknowledgement

We would like to thank Paweł Michałowski from Łukasiewicz-IMiF for performing the SIMS measurements.

References

[1] V. Šimonka, A. Hossinger, J. Weinbub and S. Selberherr, IEEE T. Electron Dev. 65 (2018) 674-679.

[2] T. Troffer, M. Schadt, T. Frank, H. Itoh, G. Pensl, J. Heindl, H.P. Strunk and M. Maier, Phys. Status Solidi A 162 (1997) 277-298.

[3] S. Asada, T. Okuda, T. Kimoto and J. Suda, Appl. Phys. Express 9 (2016) 041301.

[4] A. Parisini and R. Nipoti, J. Appl. Phys. 114 (2013) 243703.

[5] D.K. Schroder, Semiconductor Material and Device Characterization, third ed., John Wiley & Sons, New Jersey, 2006.

[6] T. Kimoto and J.A. Cooper, Fundamentals of Silicon Carbide Technology: Growth, Characterization, Devices and Applications, John Wiley & Sons, Singapore, 2014.

[7] T. Kimoto, O. Takemura, H. Matsunami, T. Nakata and M. Inoue, J. Electron. Mater. 27 (1998) 358-364.

[8] M. Lazar, C. Raynaud, D. Planson, J.-P. Chante, M.-L. Locatelli, L. Ottaviani and P. Godignon, J. Appl. Phys. 94 (2003) 2992-2998.

[9] J. Wiley and G. Miller, IEEE T. Electron Dev. 22 (1975) 265-272.

[10] A.M. Goodman, J. Appl. Phys. 34 (1963) 329-338.

[11] K. Lehovec, Appl. Phys. Lett. 26 (1975) 82-84.

[12] C. Darmody and N. Goldsman, J. Appl. Phys. 126 (2019) 145701.

[13] J. Weiße, M. Hauck, T. Sledziewski, M. Krieger, A.J. Bauer, H. Mitlehner, L. Frey and T. Erlbacher, Materials Science Forum 963 (2019) 433-436.